Energy Conversion and Management 327 (2025) 119542

Contents lists available at ScienceDirect

Energy Conversion and Management

journal homepage: www.elsevier.com/locate/enconman

Research Paper

Physics-Informed machine learning for solar-thermal power systems

Julian D. Osorio [a,*,1], Mario De Florio [a,b,*,1], Rob Hovsapian [c], Chrys Chryssostomidis [d], George Em Karniadakis [b]

[a] Center for Energy Conversion and Storage Systems, National Renewable Energy Laboratory, Golden, CO 80401, United States
[b] Division of Applied Mathematics, Brown University, Providence, RI 02912, United States
[c] Energy Systems Integration, National Renewable Energy Laboratory, Golden, CO 80401, United States
[d] Department of Mechanical Engineering, Massachusetts Institute of Technology, Cambridge, MA 02139, United States

ARTICLE INFO

Keywords:
Physics-informed machine learning
Extreme theory of functional connections
Solar-thermal power systems
Heat transfer coefficients prediction
Transient system operation

ABSTRACT

Thermal energy system modeling traditionally relies on experimental correlations to estimate heat transfer coefficients using dimensionless numbers and thermophysical properties. Multiple correlations have been proposed for different flow regimes, system geometries, and boundary conditions; however, despite their widespread use, these correlations present significant limitations related to accuracy, valid flow regime ranges, and adaptability to complex system geometries. Moreover, systems powered by intermittent renewable sources, such as solar, face added challenges due to high fluctuations in heat transfer coefficients and system variables. In this work, we change fundamentally this old paradigm. We demonstrate an experimentally validated, physics-informed machine learning approach to accurately estimate time-dependent heat transfer coefficients in solar-thermal energy systems with high variability in energy input, boundary conditions, and load. This method combines data with governing physics, providing a more accurate modeling alternative to purely data-driven frameworks and addressing the limitations of traditional experimental correlations and the need for extensive historical data for offline training. More broadly, the proposed paradigm shift can be employed in other energy plants and complex systems-of-systems.

1. Introduction

Solar-thermal power (STP) systems transform solar radiation into useful heat power. Unlike other thermal power generation systems, such as steam and gas turbines, STP technologies operate under a highly intermittent energy supply that impacts their performance and lifetime. Accurate modeling of STP systems is fundamental to evaluating their performance, defining proper and safe operational conditions, and maximizing power/heat generation [1]. Physics-based models have been used extensively to model thermal systems. However, accurate modeling of STP systems under real dynamic operation has traditionally required complex models and high computational times. Some of the main challenges to achieving accurate STP model predictions lie in the calculation of heat transfer coefficients (HTCs), which are not only difficult to measure directly in real plants, but also strongly depend on energy input characteristics, ambient conditions, and thermophysical properties [2]. HTCs are usually calculated using experimental correlations [3]. However, these correlations have limitations related to the fluid flow regime, and their applicability is delimited by a range in the dimensionless numbers (Reynolds, Prandtl, Rayleigh, and so on) describing the governing physics.

Machine learning (ML) methods are becoming an effective alternative to accurately predict the dynamic performance of thermal systems, including STP technologies [4,5]. ML methods can also help evaluate complex fluid dynamics and heat transfer phenomena involving turbulent flows [6], turbulent combustion [7], bubble growth dynamics [8], boiling heat transfer [9], interfacial thermal resistance (ITR) [10,11], and instability waves in high-speed boundary layers [12], thereby overcoming the limitations of traditional analytical and numerical methods [13].

Like HTCs, the direct measurement of ITR between two materials is challenging and usually relies on theoretical and computational methods, including the acoustic mismatch model (AMM) and the diffuse mismatch model (DMM) [14]. These models incorporate assumptions about material continuity and phonon scattering [10] that limit their prediction accuracy. Molecular dynamics models have been also proposed [14] to estimate ITR; however, these models are usually

* Corresponding authors.
E-mail address: julian.osorio@nrel.gov (J.D. Osorio).
[1] First and second authors contributed equally to this work.

https://doi.org/10.1016/j.enconman.2025.119542
Received 6 December 2024; Received in revised form 16 January 2025; Accepted 17 January 2025
Available online 27 January 2025

Nomenclature

T_t	Tank temperature, K
T_1	Temperature outflow tank/inflow solar collector, K
T_2	Temperature outflow solar collector/inflow tank, K
T_3	Temperature outflow tank/inflow heat exchanger, K
T_4	Temperature outflow heat exchanger/inflow tank, K
T_c	Mean fluid temperature inside solar collectors, K
T_s	Temperature of solar absorber internal surface, K
T_∞	Ambient temperature, K
T_W	Temperature of the tank external surface, K
$\dot{Q}_{in}$	Heat absorbed by the heat transfer fluid, W
$\dot{Q}_{l,c}$	Heat loss in the solar collector, W
$\dot{Q}_{lk}$	Heat leak Rankine cycle, W
$\dot{Q}_{max}$	Maximum heat transfer in the thermal engine, W
$\dot{W}_{RC}$	Net power output Rankine cycle, W
$\dot{m}_c$	Mass flow rate inside the solar collectors, kg s^{-1}
$\dot{m}_{RC}$	Mass flow rate Rankine cycle, kg s^{-1}
h_0	Heat transfer coefficient fluid/absorber, $Wm^{-2}k^{-1}$
h_{air}	Heat transfer coefficient tank/ambient, $Wm^{-2}k^{-1}$
U_t	Overall heat transfer coef. tank/ambient, $Wm^{-2}k^{-1}$
k_t	Thermal conductivity tank shell, $Wm^{-1}k^{-1}$
k_f	Thermal conductivity heat transfer fluid, $Wm^{-1}k^{-1}$
k_{air}	Thermal conductivity air, $Wm^{-1}k^{-1}$
c_p	Specific heat of the heat transfer fluid, J $kg^{-1}k^{-1}$
ρ_f	Density of the heat transfer fluid, kg m^{-3}
μ	Viscosity of the heat transfer fluid, kg $m^{-1}s^{-1}$
μ_0	Viscosity of the fluid evaluated at T_W, kg $m^{-1}s^{-1}$
I	Direct normal irradiance, $W/m^{-2}(-\|\text{-})$
V_{wind}	Average wind speed, m/s
$Load$	Electric load, W
A_t	Surface area of the tank, m^2
A_{int}	Internal surface area of the solar absorber, m^2
A_c	Aperture area solar collectors, m^2
V_c	Volume of the absorber pipe, m^3
V_t	Tank volume, m^3
D	Tank diameter, m
r_t	Tank radius, m
t_t	Thickness of tank insulation layer, m
t	Time, s
f	Friction factor
η_{eq}	Equivalent efficiency
SoC	State of charge
τ	Ratio cold/hot input reservoir temperature
τ_H	Ratio hot temperatures engine/reservoir
rM	Effective conductance ratio
Re	Reynolds number
Re_D	Reynolds number based on diameter
Pr	Prandtl number
Pr_0	Prandtl number evaluated at T_W
Z	Constant parameter Eq. (8)
m	Exponent Eq. (8)
n	Exponent Eq. (8)
C	Constant coefficient Eq. (9)

Physics Informed Machine Learning

y	Differential equation's solution
y_0	Differential equation initial condition
$\dot{y}$	Derivative of differential equation's solution
β	Neural network output weights
$\boldsymbol{g}$	TFC free-chosen function
σ	Neural network activation function
$\boldsymbol{J}$	Jacobian matrix of loss functions with respect to unknown parameters
$U_{t,r}$	Real heat transfer coefficient, $Wm^{-2}k^{-1}$
$U_{t,p}$	Predicted heat transfer coefficient, $Wm^{-2}k^{-1}$

Acronyms

AMM	Acoustic mismatch model
DMM	Diffuse mismatch model
DNI	Direct normal irradiance
GRU	Gated recurrent unit
HTC	Heat transfer coefficient
HTF	Heat transfer fluid
ITR	Interfacial thermal resistance
IVP	Initial value problem
ML	Machine learning
PTC	Parabolic trough collector
STP	Solar-thermal power
TFC	Theory of functional connections
X-TFC	Extreme Theory of Functional Connections

computationally expensive and rely on empirical interatomic potential functions that could impact the prediction accuracy [10]. ML methods, in contrast, have been demonstrated to be highly effective in determining and forecasting ITR behavior; they also have high accuracy and low computational cost, outperforming the conventional AMM and DMM methods [10,11]. Although ML has been used successfully in the context of ITR, it has not been used to estimate HTCs in thermal systems under dynamic operation.

In this study, we developed a physics-informed machine learning framework based on the Extreme Theory of Functional Connections (X-TFC) algorithm [15] to accurately determine the evolution of performance parameters and HTCs in STP systems as a function of variable solar radiation, air temperature, wind speed, and electric load. X-TFC allows for analytical satisfaction of the problem constraints (i.e., initial condition), and it leverages random-projection neural networks and domain decomposition [16] trained with time-series data and differential equations. To evaluate the effectiveness of the X-TFC method, the initial analysis considered a physics-based model of an STP system that used HTCs calculated with broadly accepted experimental correlations. Then, the new framework was employed to predict the HTC between a molten salt thermal energy storage tank and the environment using real data from a concentrating solar power plant. We found that the X-TFC framework outperformed state-of-the-art, data-driven methods such as gated recurrent unit (GRU) and transformers in terms of accuracy and computational time, without the need for offline training with historical data. This demonstrates the advantage of the proposed ML approach in predicting HTCs, performance indicators, and other thermal system variables.

2. Methods

2.1. Physics-based model for the STP system

The STP system analyzed consists of parabolic trough collectors (PTCs) and a Rankine cycle connected through a thermal energy storage tank (Fig. 1a). The physics-based model was developed by analyzing these three main components. The energy balance equation for the PTC absorber can be expressed as follows:

$$\frac{dT_c}{dt} = \frac{h_0 A_{int}}{\rho_f V_c c_p}(T_s - T_c) + \frac{\dot{m}_c}{\rho_f V_c}(T_t - T_2) - \frac{\dot{Q}_{l,c}}{\rho_f V_c c_p} \tag{1}$$

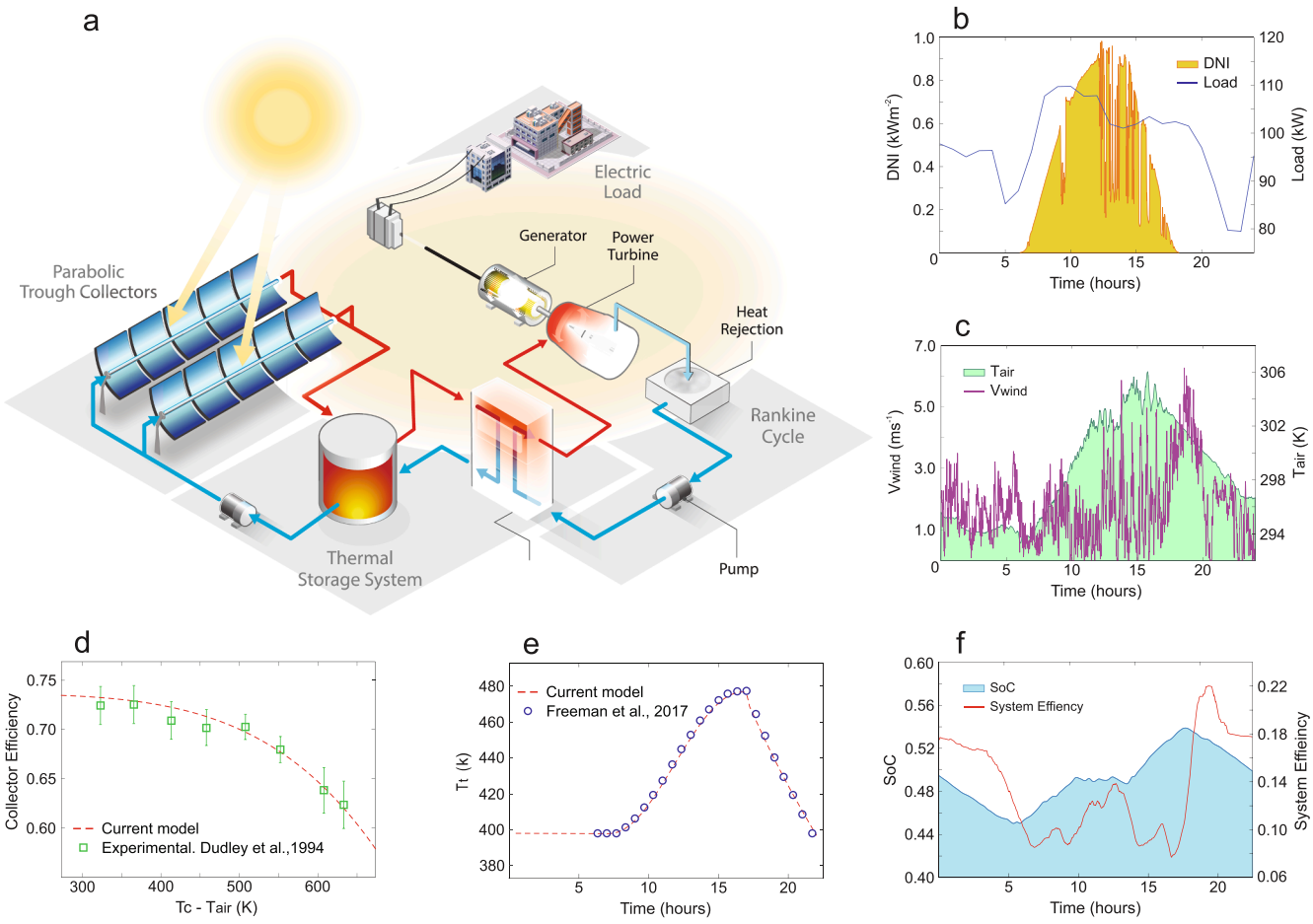

Fig. 1. (a) Solar-thermal systems operate under highly variable conditions due to the intermittent nature of (b) solar radiation and electric load and (c) air temperature and wind speed. Their dynamic operation leads to intermittent operating variables and heat transfer coefficients, which are challenging to estimate accurately through modeling or experiments. (d) and (e) Solar-thermal system model validation. (f) Thermal energy storage state-of-charge (SoC) and system efficiency for one day of operation under variable direct normal irradiance (DNI), wind velocity, air temperature, and load.

where T_c [K] is the mean temperature of the heat transfer fluid (HTF) inside the solar collector, t [s] is the time, A_{int} [m^2] is the internal surface area of the absorber, ρ_f [kg m^{-3}] is the HTF density, V_c [m^3] is the absorber pipe volume, c_p [J kg^{-1}k^{-1}] is the specific heat of the HTF, T_s [K] is the internal surface temperature of the absorber pipe, $\dot{m}_c$ [kg s^{-1}] is the mass flow rate, $\dot{Q}_{l,c}$ [W] is the heat loss, and T_t [K] and T_2 [K] are the collector inlet (tank temperature) and outlet temperatures, respectively. The first and second terms on the right side of Eq. (1) correspond to the heat absorbed and then transferred to the HTF, $\dot{Q}_{in} = h_0 A_{int}(T_s - T_c)/\rho_f V_c c_p$ [W] and the net energy of the HTF flow, respectively. $\dot{Q}_{in}$ and $\dot{Q}_{l,c}$ are respectively calculated from an optical and a thermal analysis using the proposed PTC model by Osorio et al. [17], and h_0 [Wm^{-2}k^{-1}] is the convection HTC between the absorber's internal surface and the HTF. Three experimental correlations are considered in this work to determine h_0 : Gnielinski [18] (Eq. (2), Dittus-Boleter [19] (Eq. (4), and Sieder-Tate [20] (Eq. (5). Additional details for the physics-based model are presented in Appendix A.

$$h_0 = \frac{k_f}{D}\frac{\left(\frac{f}{8}\right)(Re-1000)Pr}{1+12.7\sqrt{\left(\frac{f}{8}\right)}\left(Pr^{2/3}-1\right)}\left(\frac{Pr}{Pr_0}\right)^{0.11} \tag{2}$$

The Gnielinski correlation is valid for $3000 \leq Re \leq 5e6$ and $0.5 \leq Pr \leq 2000$. The friction factor for the inner surface of the absorber, f, is calculated as follows [21]:

$$f = [0.790ln(Re) - 1.64]^{-2} \tag{3}$$

$$h_0 = \frac{k_f}{D}0.023Re^{0.8}Pr^{0.4} \tag{4}$$

$$h_0 = \frac{k_f}{D}0.027Re^{0.8}Pr^{1/3}\left(\frac{\mu}{\mu_0}\right)^{0.14} \tag{5}$$

In Eqs. (2), (4), and (5), k_f [Wm^{-1}k^{-1}] is the thermal conductivity of the HTF (SYLTHERM 800 was selected for this study), D [m] is the internal diameter of the absorber, Re is the Reynolds number, Pr is the Prandtl number evaluated at the temperature of the HTF, and Pr_0 is the Prandtl number evaluated a the absorber temperature. In Eq. (5), μ is the viscosity evaluated at the fluid temperature, while μ_0 is the viscosity evaluated at the wall temperature.

Similarly, the energy balance for the thermal energy storage tank yields:

$$\frac{dT_t}{dt} = \frac{\dot{m}_c}{\rho_f V_t}(T_2 - T_t) - \frac{\dot{m}_{RC}}{\rho_f V_t}(T_t - T_4) - \frac{A_t U_t (T_t - T_\infty)}{\rho_f V_t c_p} \tag{6}$$

For periods when there is no inflow and outflow, the temperature change in the tank is only governed by the heat loss to the environment:

$$\frac{dT_t}{dt} = -\frac{A_t U_t (T_t - T_\infty)}{\rho_f V_t c_p} \tag{7}$$

where T_t [K] is the temperature of the HTF inside the tank (or tank temperature), V_t [m^3] is the tank volume, $\dot{m}_{RC}$ is the mass flow rate [kg s^{-1}] of the fluid in the Rankine cycle, and T_4 [K] is the temperature of water entering the tank after passing through the heat exchanger. The last term in Eq. (6) corresponds to the heat loss in the tank, where U_t [$Wm^{-2}K^{-1}$] and A_t [m^2] correspond to the overall HTC between the tank and the environment and the tank's surface area, respectively, and T_∞ [K] is the ambient temperature. Three experimental correlations were also used in this study to calculate the convection HTC between the tank and the environment (h_{air}): Zukauskas [22] (Eq. (8)), Hilpert [23] (Eq. (9)), and the Churchill-Bernstein correlation [24] (Eq. (10)):

$$h_{air} = \frac{Zk_{air}Re_D^m Pr^n}{2r_t}\left(\frac{Pr}{Pr_0}\right)^{1/4} \tag{8}$$

$n = 0.37$ for $Pr < 10$, $n = 0.36$ for $Pr > 10$

$$h_{air} = \frac{Ck_{air}Re_D^m Pr^{1/3}}{2r_t} \tag{9}$$

$Pr > 7.0$

$$h_{air} = \frac{k_{air}}{2r_t}\left\{0.3 + \frac{0.62Re_D^{1/2}Pr^{1/3}}{\left[1+(0.4/Pr)^{2/3}\right]^{1/4}}\left[1+\left(\frac{Re_D}{282,000}\right)^{5/8}\right]^{4/5}\right\} \tag{10}$$

$Re_D Pr > 0.2$

In Eqs. (8), (9), and (10), k_{air} [$Wm^{-1}k^{-1}$] is the thermal conductivity of the air, r_t [m] is the tank radius, and C, Z, m, and n are constants [2] that depend on the flow characteristics. U_t as a function of h_{air} is then calculated using a thermal resistance approach for the thermal energy storage tank, which is treated as a cylinder with thickness t_t [m]:

$$U_t = \frac{h_{air}k_t}{k_t + h_{air}(r_t+t_t)^* ln\left(\frac{r_t+t_t}{r_t}\right)} \tag{11}$$

For the molten salt tank, U_t is calculated using a similar approach considering a multilayer cylinder composed of a metallic shell, an intermediate magnesium, and a mineral wool insulation layer.

The model for the Rankine cycle was developed using an endoreversible engine approach that considered finite heat transfer rates between the heat engine and the hot and cold reservoirs, which are modeled as variable temperature heat sources. The model also considered irreversibilities associated with the expansion and compression processes through an equivalent efficiency (η_{eq}). The efficiency of the Rankine cycle using this approach is expressed as follows [25]:

$$\eta_{RC} = \frac{\eta_{eq}(1-\tau_H)[rM\tau_H + \tau_H - rM\tau - 1]}{\left[(1-\tau_H) + \left(\frac{\dot{Q}_{lk}}{\dot{Q}_{max}}\right)^{\frac{(rM+1)(1-\tau)}{4}}\right]\left[\tau_H(rM+\eta_{eq}) - \eta_{eq}\right]} \tag{12}$$

where τ corresponds to the ratio between the cold and hot input reservoir temperatures, and τ_H is defined as the ratio between the hot side engine and hot input reservoir temperatures. Both τ and τ_H depend on the tank temperature T_t. A value of $\dot{Q}_{lk} = 0.01^*\dot{Q}_{max}$ is considered in this study, where $\dot{Q}_{max} = (UA)_{eq}(T_t - T_\infty)$. The parameter rM corresponds to an effective conductance ratio between dissipation and input heat exchangers. Additional details for the calculation of rM and η_{eq} are presented in the Appendix.

Finally, the efficiency of the STP system is defined as the ratio between the power output in the Rankine cycle ($\dot{W}_{RC}$) and the solar energy input (IA_c) and the decrease/increase in the stored energy in the tank ($\rho_f V_t c_p \frac{dT_t}{dt}$) [4] as follows:

$$\eta = \frac{\dot{W}_{RC}}{IA_c - \rho_f V_t c_p \frac{dT_t}{dt}} \tag{13}$$

where I [Wm^{-2}] is the direct normal solar irradiance (DNI) and A_c [m^2] is the solar collector aperture area.

2.2. Data acquisition

The direct normal solar irradiance $I(t)$, the ambient temperature $T_\infty(t)$, the average wind speed $V_{wind}(t)$, and an electric load $Load(t)$ imposed on the Rankine cycle are the input parameters for the solar thermal system model. These parameters are provided at 1-minute resolution. The corresponding input parameter profiles for the analyzed days are presented in Fig. 4e to 4 h. I, T_∞, and V_{wind} were measured in 1-minute resolution at the National Renewable Energy Laboratory's (NREL's) Solar Radiation Research Laboratory in Golden, Colorado (latitude: 39.742° north, longitude: 105.182° west [26]) from August 1–7, 2021. The electric load imposed on the power generation system corresponds to a typical manufacturing profile for one week [27].

2.3. Physics-informed neural networks

To retrieve $U_t(t)$ as a function of time, given the time-series data that represent the evolution of the tank temperature (T_t), we developed a physics-informed neural network framework using the X-TFC algorithm for gray-box model identification. We represent the solution of the differential equation with a so-called constrained expression provided by the Theory of Functional Connections (TFC) [15,28]. According to the TFC, the constrained expression for his constrained problem is built as:

$$y(t,\beta) = \boldsymbol{g}(t,\beta) - g(0,\beta) + y_0 \tag{14}$$

such that the constrained problem is turned into an unconstrained problem. Here, $g(t,\beta)$ is an arbitrarily chosen function, for which the constrained expression will always analytically satisfy the initial condition y_0. According to the X-TFC framework, the function $g(t,\beta)$ is selected to be a random-projection shallow neural network with randomly distributed input weights and biases, as follows:

$$\boldsymbol{g}(t,\beta) = \sum_{j=1}^{L}\beta_j\sigma(w_j t + b_j) = \boldsymbol{\sigma}^T\beta \tag{15}$$

where $j = 1,\ldots,L$ refers to the j^{th} neuron of the neural network hidden layer, β is the vector of the output weights (unknown) of each neuron, and w_j and b_j are their input weights and biases (randomly initialized with a uniform distribution). Thus, the constrained expression and its derivative have the following form:

$$y(t,\beta) = \left[\sigma - \sigma_0\right]^T\beta + y_0 \tag{16}$$

$$\dot{y}(t,\beta) = \dot{\sigma}^T\beta \tag{17}$$

where $\sigma(t)$ and $\sigma(0)$ are referred as σ and σ_0, for simplicity. Because the time domain of the STP system can be very large (days to months), a time-domain decomposition is performed by dividing the domain into n subintervals of the same length, $h = t_k - t_{k-1}$, for $k = 1,\ldots,n$. Thus, our initial value problem (IVP) turns into a composition of multiple consecutive IVPs of the form $\frac{dy^{(k)}}{dt} = f(y^k, t)$ with initial conditions $y(0)^{(k)} = y_0{}^{(k)}$. Then, the X-TFC algorithm is applied iteratively for each subdomain, with a continuity condition $y_0{}^{(k)} = y_f{}^{(k-1)}$ imposed at each interface.

The physics-based model under study characterizes the evolution in time of T_t and is described by Eq. (6). The h_0 term in Eq. (1) and the U_t term in Eq. (6) are learned using the X-TFC framework.

The loss functions to be minimized in the training process are the differential equation residual loss (L_{T_t}) and the data loss (L_{data}):

$$L_{T_t} \equiv \frac{dT_t}{dt} - \frac{\dot{m}_c}{\rho_f V_t}(T_2 - T_t) + \frac{\dot{m}_{RC}}{\rho_f V_t}(T_t - T_4) + \frac{U_t A_t}{c_p \rho_f V_t}(T_t - T_\infty) \quad (18)$$

$$L_{data} \equiv \widehat{T}_t - T_t \quad (19)$$

where $\widehat{T}_t$ is the observed data of the tank temperature in time. To solve this nonlinear system of equations, we first compute a Jacobian matrix by differentiating the loss functions with respect to the unknown weights β, as follows:

$$J = \left[\frac{\partial L_{T_t}}{\partial \beta_T}, \frac{\partial L_{T_t}}{\partial \beta_U}; \frac{\partial L_{data}}{\partial \beta_T}, \frac{\partial L_{data}}{\partial \beta_U}\right] \quad (20)$$

The unknown vector β is computed with an iterative least-square algorithm that solves the system $\boldsymbol{J}\Delta\boldsymbol{\beta}^k = \boldsymbol{L}$, where $\boldsymbol{L} = [L_{T_t}; L_{data}]$ is the vector containing the loss functions and minimizing the value of the norm $\left(\boldsymbol{J}\Delta\boldsymbol{\beta}^k - \boldsymbol{L}\right)$. Each k^{th} iteration corresponds to an update of the output weights $\beta^{k+1} = \beta^k + \Delta\beta^k$, where:

$$\Delta\beta^k = -(J^T(\beta^k)J(\beta^k))^{-1}J^T(\beta^k)L(\beta^k) \quad (21)$$

After the output weights β_T and β_U are trained to minimize the loss functions, they are replaced in the constrained expression for T_t and in the neural network representation of U_t. The schematic of the overall X-TFC framework is shown in Fig. 3.

2.4. Heat transfer coefficient estimation

The heat transfer coefficient h_0 for the solar-thermal collector is estimated with the physics-data-driven X-TFC framework by leveraging the physics knowledge of the energy balance differential (Eq. (1)) as well as the available collected data for the tank temperature, T_t;, the mean temperature of the HTF inside the collector, T_c; the specific heat of the HTF, c_p; the internal surface temperature of the absorber pipe, T_s; the HTF density,ρ_f; the mass flow rate $\dot{m}_c$, and the heat loss $\dot{Q}_{loss}$. In our simulations, we consider one daylight time range when the solar collector is operative. Our framework is set with 10 neurons and 10 collocation points for each 1-second subdomain. The learned HTC versus the real HTC data is plotted in Fig. 4a for 7 days of plant operation. The performance of the HTC estimation is evaluated with the relative error, by comparing the real ($U_{t,r}$) and the predicted ($U_{t,p}$) heat transfer coefficients, as follows:

$$Relative\ Error(\%) = \frac{|U_{t,r} - U_{t,p}|}{U_{t,r}} x100 \quad (22)$$

The first simulation uses 1 week of collected time-series data, and X-TFC is used to estimate U_t. The accuracy of this estimate overlaps with the exact value obtained from the forward model using the Zukauskas correlation [22]. The time domain is decomposed into subintervals of 60 s each, in which X-TFC is iteratively employed, using 10 collocation points and 10 neurons, with the iterative least-square tolerance set to 1e-9. The overall computational time to estimate the U_t coefficient for the entire week is on the order of about 10 s on Intel® Xeon® W-2255 (19.25 MB cache, 10 cores, 20 threads, 3.70 GHz to 4.70 GHz Turbo, 165 W) Processor. The perfect overlap between the learned and observed tank temperature, and between the estimated and exact U_t coefficient, can be qualitatively seen in Fig. 4a. The relative error for the U_t coefficient estimation is reported in the second plot (Fig. 4c), showing values between 10^{-10} % and 10^{-2} %.

With the same approach, we aim to estimate the efficiency of the collector (Eq. A(3) in Appendix A) during its daily operation for 7 days. We use a time step of 60 s, 10 collocation points for each step, and 35 neurons, with an iterative least-square tolerance of 1e-09, for an overall computational time of 15 s. In Fig. 5a, the learned efficiency is plotted against the nominal value, showing a relative error on the order of 1 % in Fig. 5b.

2.5. ML models implementation

The GRU model was implemented with 10 layers, each containing 100 hidden units, and was trained over 5000 epochs with a learning rate of 0.001. The training process required 140 s, resulting in a training L2 loss of 1.2e-5. The Transformer model, with five layers and four attention heads, was also trained for 5000 epochs at a learning rate of 0.001. This model took 275 s to train, yielding a training L2 loss of 3.5e-4. The X-TFC method, configured with 10 collocation points and 10 neurons per 60-second time step, required only 1 s of overall computational time performed on CPU. With an iterative least-square process capped at 100 iterations and a tolerance of 1e-9, X-TFC achieved a significantly lower training L2 loss of 8.5e-17.

3. Performance evaluation of a solar-thermal power system

STP systems are designed to convert solar energy into useful heat to drive a power generation cycle. Fig. 1a shows a solar-thermal system configuration that uses PTCs to concentrate solar radiation during daylight and transfer it to a fluid such as water or thermal oil. The hot fluid is routed to a thermal energy storage tank to increase the temperature of the fluid inventory (charging) through mixing. The energy stored in the tank is extracted (discharging) to drive the power generation cycle. Concentrating STP systems operate under highly variable conditions due to the alternating nature of direct normal irradiance (DNI), wind speed (V_{wind}), changes in the air temperature (T_∞), and variable electric loads when connected to the electric grid/microgrid (see Fig. 1b and 1c). The developed physics-based model for the STP system was validated using experimental data and other validated models available in the literature [29,30] (Fig. 1d and 1e). The model was used to determine the system performance by calculating the state of charge (SoC) and efficiency (Fig. 1f) under dynamic operation conditions.

Evaluating the system performance requires estimating HTCs, which are usually computed through experimental correlations based on the thermophysical properties of the working fluid, component characteristic dimensions, and measurable quantities such as temperature. The internal HTC (h_0) between the absorber pipe in the PTC and the working fluid (SYLTHERM 800) is necessary to determine the solar radiation absorbed by the HTF in the solar collector. It was calculated using three well-known correlations proposed by Gnielinski [18], Dittus-Boleter [19], and Sieder-Tate [20] (Fig. 2a). Significant differences in h_0 were obtained during 18 h of operation, depending on the selected correlations; differences of up to 3.1 $kWm^{-2}K^{-1}$ (18.6 %) and 7.2 $kWm^{-2}K^{-1}$ (33.5 %) were respectively obtained using the Dittus-Boelter and Sieder-Tate correlations, compared with the h_0 calculated using the Gnielinski correlation. Similarly, to determine the thermal losses, we computed the overall external HTC (U_t) between the storage tank and the environment using three accepted correlations proposed by Zukauskas [22], Hilpert [23], and Churchill-Berstein [24] (Fig. 2b). In these cases, h_0 was computed with the Gnielinski correlation. Using the Hilpert or Churchill-Berstein correlation leads to an overestimation of U_t of up to 0.23 $Wm^{-2}K^{-1}$ (20.6 %) or 1.27 $Wm^{-2}K^{-1}$ (505.0 %), respectively, with respect to the U_t calculated using Zukauskas correlation.

Fig. 2c and 2d present the prediction of the system efficiency and tank temperature (T_t), respectively, using the three different correlations for U_t and the Gnielinski correlation for the h_0 calculation. Significant differences in the system efficiency and T_t are observed. It has been demonstrated that the use of different correlations to determine heat transfer has a strong impact on the system evaluation. This could be even more important for systems operating under variable regimes, for instance solar and wind, leading to highly variable HTCs. In addition to the intrinsic uncertainty in the system performance evaluation

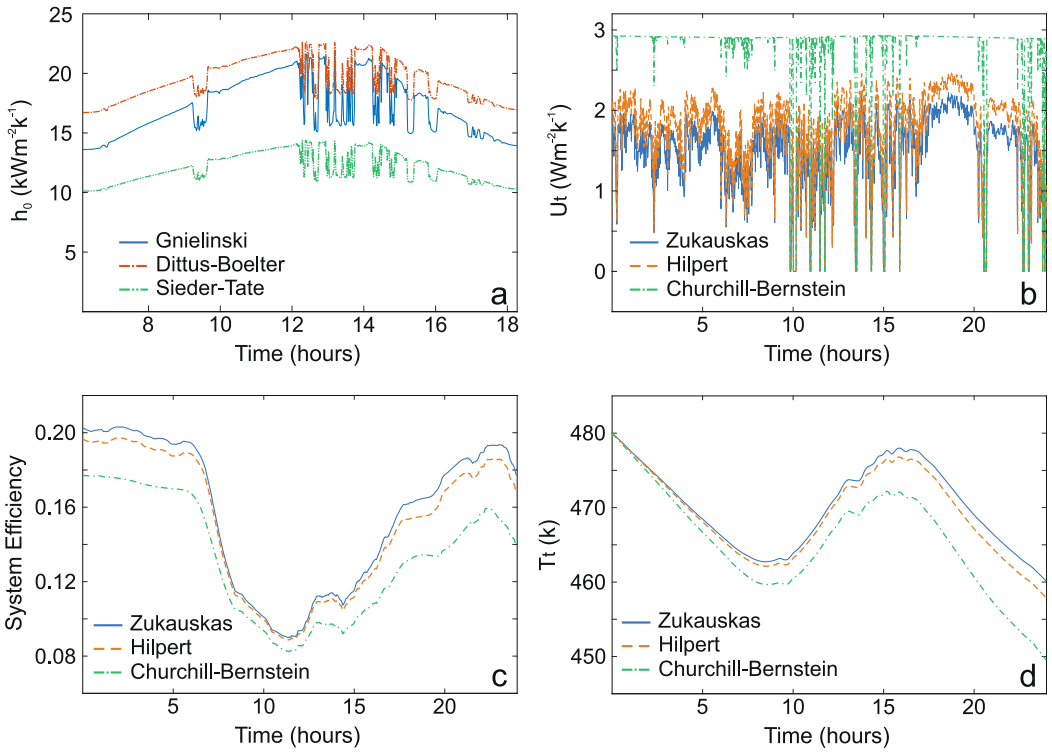

Fig. 2. Significant differences in the estimation of heat transfer coefficients are obtained using different well-known and accepted experimental correlations. Impact of using different correlations to determine (a) the internal heat transfer coefficient h_0, (b) the external overall heat transfer coefficient U_t, (c) the system efficiency, and (d) the tank temperature T_t.

associated with the use of experimental correlations, most of these correlations also present limitations in the range of dimensionless variables (i.e., Reynolds, *Re*; Prandtl, *Pr*; Rayleigh, *Ra*, …) where they are applicable. To improve the accuracy of the HTC calculation and the system performance evaluation, we developed a novel ML framework based on the X-TFC method [15]. This new framework not only addresses the accuracy limitations of experimental correlations, but also performs very well under highly variable regimes without any restriction on the values of Reynolds (*Re*), Prandtl (*Pr*), Rayleigh (*Ra*), or any other dimensionless number or quantity.

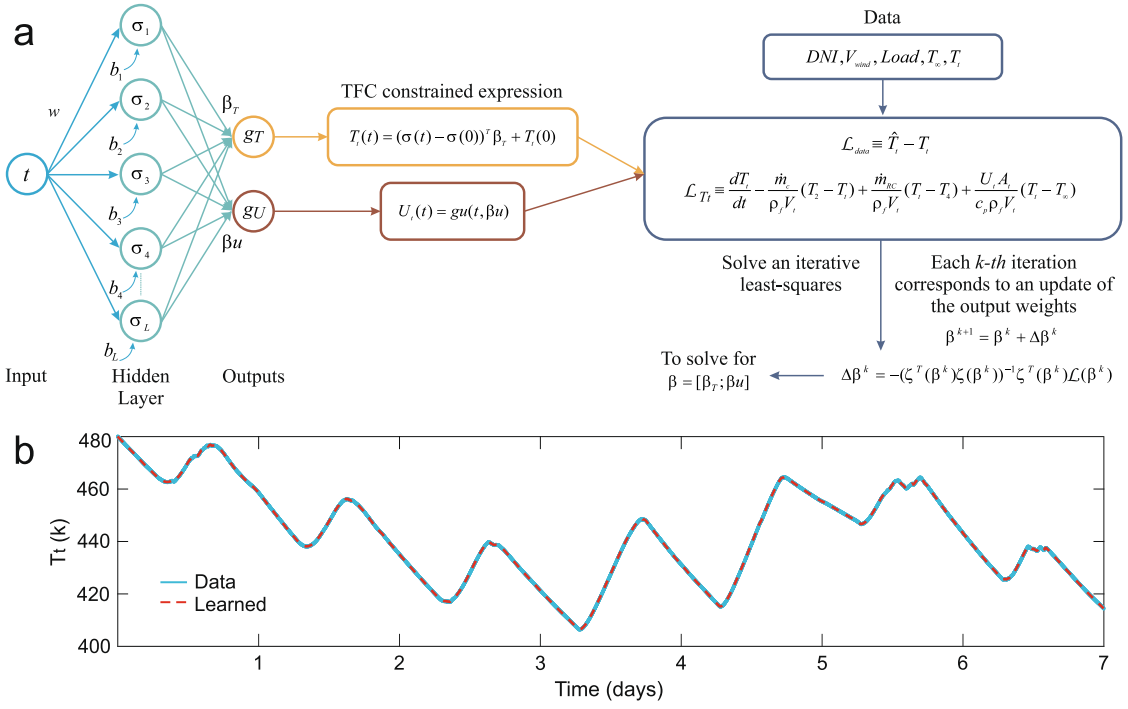

Fig. 3. The Extreme Theory of Functional Connections framework effectively solves the differential governing equations and accurately predicts system temperatures, performance variables, and heat transfer coefficients. (a) Physics-data-driven X-TFC framework that allows an accurate (b) prediction of the system operation.

4. Machine learning framework development based on X-TFC

We use the X-TFC method to solve the differential governing equations for the STP system (Eqs. (1) and (2)) using a gray-box model identification approach [31,32] with a so-called constrained expression, such that the constrained problem is turned into an unconstrained problem. An X-TFC formulation for the governing energy balance for the storage tank (Eq. (1)) to determine U_t is schematically presented in Fig. 3a. A similar formulation is implemented in the X-TFC framework to predict the evolution in time of any system variable—including efficiency, SoC, and h_0—using time-series data that represent the evolution of T_t, which is learned by X-TFC (Fig. 3b).

5. System performance evaluation and uncertainty quantification

The physics-based model is used to determine the evolution of the temperature of the HTF inside the tank, the temperature of the fluid at the solar collector outlet (T_2), and the temperature of the fluid returning to the tank after passing through the heat exchanger (T_4) (Fig. 1a). Under good mixing conditions, the temperature of the fluid leaving the tank toward the primary heat exchanger (T_3) and the solar collector (T_1) must be similar to T_t, i.e., $T_t \approx T_1 \approx T_3$. The physics-based model used Zukauskas and Gnielinski correlations to calculate the HTCs. These HTCs were then used to determine the system temperatures that conform to the dataset used in the X-TFC framework, which in turn enable us to estimate U_t, h_0, SoC, and efficiency. In this initial approach, we used the synthetic data obtained from the physics-based model to evaluate the accuracy and efficacy of the X-TFC framework. However, for real plant applications, the synthetic dataset could be replaced by real temperature measurements that will serve as input to the X-TFC framework to determine U_t, h_0, or any other system variable without the assistance of any experimental correlation.

The estimated time-dependent U_t and h_0 functions obtained from the X-TFC framework are presented in Fig. 4a and 4b, respectively, and compared with the corresponding functions calculated via the physics-based model. Large fluctuations in DNI, V_{wind}, T_∞, and load lead to highly-variable temperatures and HTCs (Fig. 4e–4 h). Even under these conditions, the X-TFC framework is capable of predicting U_t for 7 days and h_0 for 1 day within just a few seconds of computational time. This enables a scale-up of system evaluation for months of operation under reasonable computational times. Other ML frameworks based on deep neural networks usually require longer computational times for back-propagation computation to conduct parameter optimization, making simulations impractical for systems with long operation times [33,34]. It is worth noting that high-frequency signals or domains, like solar systems operating under variable DNI and climatic conditions, are usually difficult to predict using ML techniques. Often, system properties and variables with high frequency are approximated as constant parameters to facilitate their treatment [35]. The X-TFC framework demonstrated high capacity to capture the variable fluctuations with high accuracy, obtaining relative errors below 0.01 % for U_t in almost the entire 7-day operation range (Fig. 4c) and relative errors below 10 % for h_0 for 1-day operation (Fig. 4d).

We also assessed the capability of the X-TFC framework to predict other system variables, including the system efficiency (Eq. (17). Like the HTCs, the X-TFC is very useful for predicting diverse system parameters and variables that are difficult to measure or cannot directly be measured in real thermal energy conversion systems. Fig. 5 demonstrates the accurate prediction of the system efficiency during the analyzed time span of 7 days with maximum relative errors below 10 %.

X-TFC is a physics-informed method that does not require offline

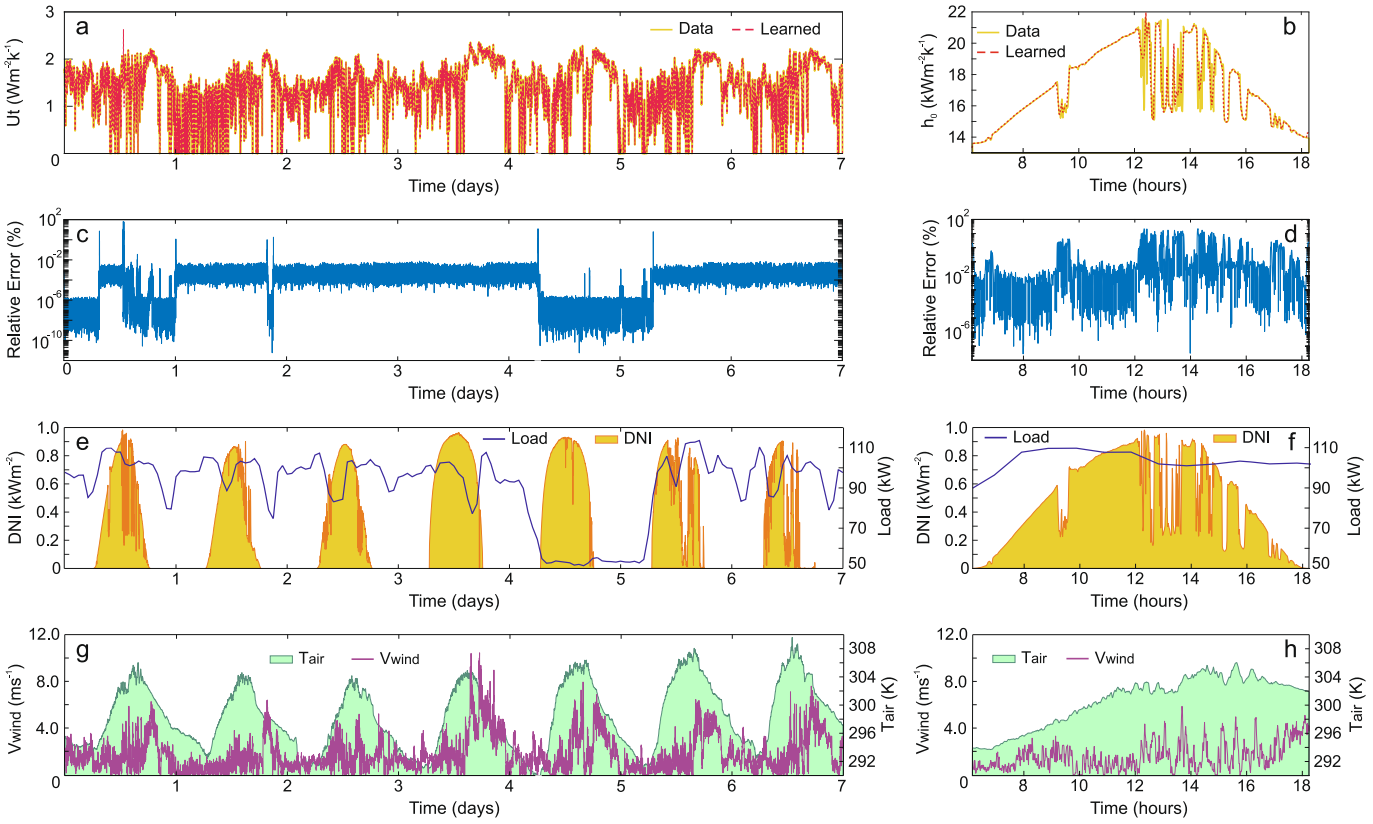

Fig. 4. Heat transfer coefficients for (a) external and (b) internal flows are accurately estimated by the X-TFC method in solar-thermal power systems operating under highly variable conditions. (c) Relative errors below 0.01% for U_t and (d) 10% for h_0 are obtained, when compared with the data calculated with the STP physics-based model. System operation conditions used in the prediction and model calculations included (e) and (f) direct solar radiation and electric load and (g) and (h) average wind speed and ambient temperature profiles.

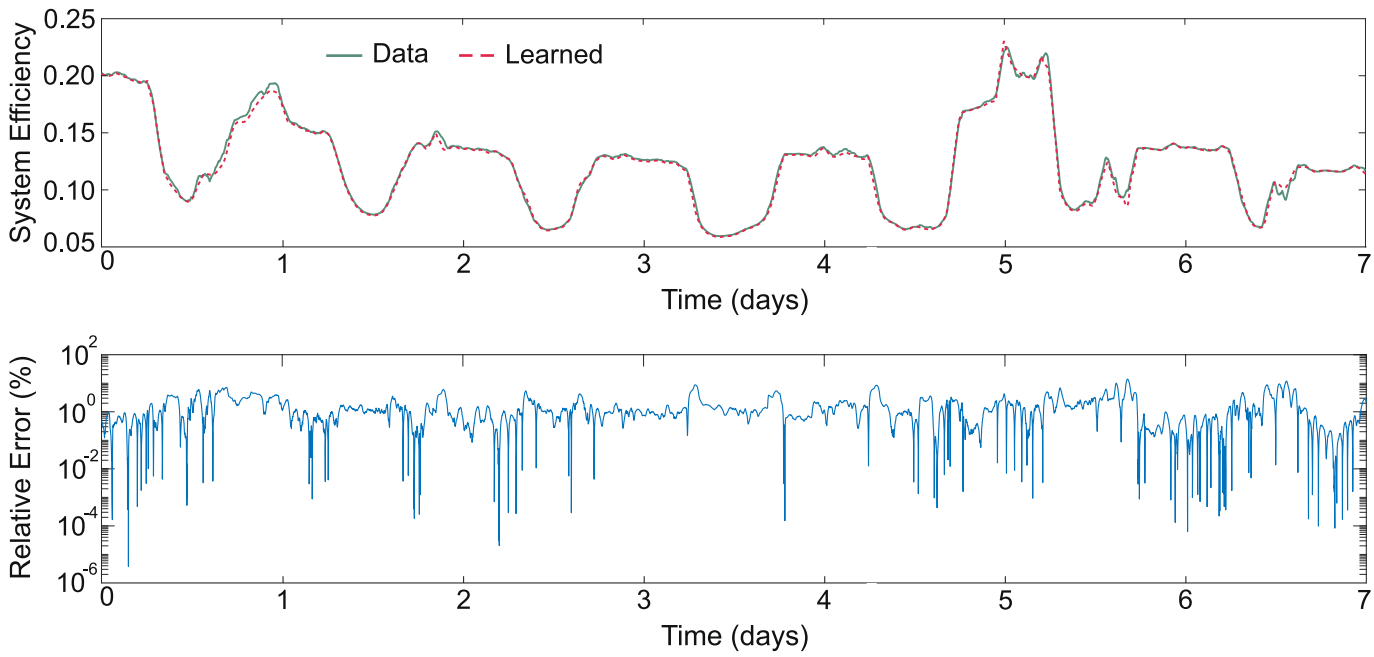

Fig. 5. The X-TFC framework effectively and accurately predicts other system variables like (a) thermal efficiency during a 7-day operation under the intermittent conditions presented in Fig. 4e and 4g. (b) Maximum relative errors below 10 % in the efficiency calculation are obtained using X-TFC when compared with the efficiency calculated with the physics-based model.

training or prior knowledge of the unknown variables, usually enabling a faster solution than data-driven methods. We compared the performance of the X-TFC to two conventional and accurate data-driven methods: gated recurrent unit (GRU) [36] and transformers [37]. The U_t function for the STP system was predicted with these three methods for the first 24 h of operation, considering the four variable inputs presented in Fig. 4e and 4 g: DNI, V_{wind}, T_∞, and load. The U_t predictions for the three methods are presented in Fig. 6 (top plots) with the respective relative errors (bottom plots). The figure shows that the behavior of U_t was accurately learned for all three methods; however, a significant difference in the relative errors was obtained. Both GRU and transformers led to relative errors ranging between 0.1 % and 10 %, whereas the X-TFC relative errors ranged between 1e-7 % and 1e-3 %, demonstrating a higher accuracy. The X-TFC method was approximately 140 times faster than GRU and 275 times faster than transformers. GRU and transformer models were run on GPU NVIDIA® RTXTM A5000, 24 GB GDDR6, 4DP.

As demonstrated, the X-TFC framework can be used to directly

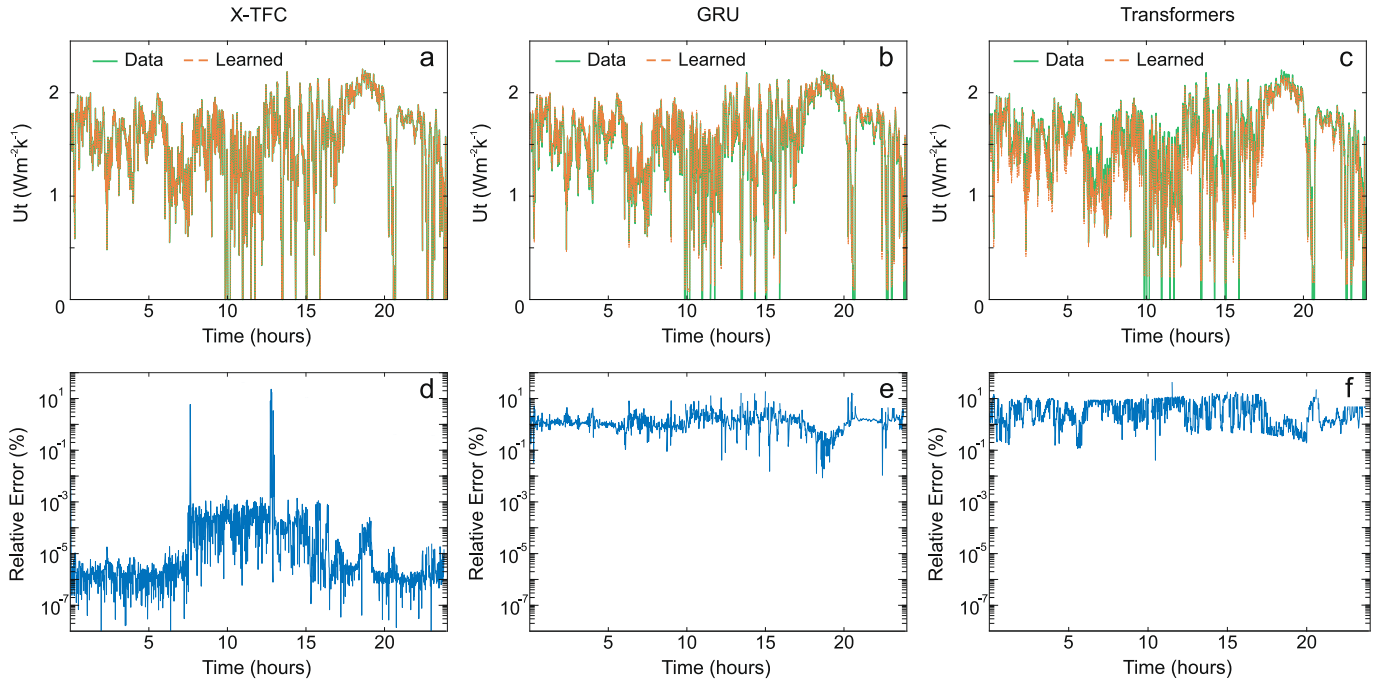

Fig. 6. (a) – (c) The proposed X-TFC framework outperforms other conventional and accurate data-driven methods, such as GRU and transformers, in the calculation of heat transfer coefficients. (d) Relative errors between 1e-7% and 1e-3% were obtained with X-TFC in almost the entire 24-hour operation range analyzed. (e) and (f) Relative errors between 0.1% and 10% were obtained with GRU and Transformers.

determine HTCs and other thermal system variables with high accuracy using data that can be obtained from real measurements using sensors. Temperature, pressure, volumetric flow, fluid level, and valve position, among other variables, are usually measured and collected in thermal plants to monitor the system operation, analyze behavior trends, identify abnormal operation or malfunction, and/or forecast a particular system variable. These field measurements, even when they have associated uncertainty, are a valuable source of information that could be used to train neural networks to discover the underlying physics of the system. They could serve multiple purposes, from system performance evaluation to plant operation maximization.

Validation with real data: To validate the efficacy of the proposed ML framework, we used *real data* from a molten nitrate salt thermal energy storage tank of a 50-MW concentrating solar power plant [38]. The data consisted of a set of temperatures collected at a 1-hour resolution from 10 thermocouples located inside the 21-m-diameter tank. The analysis was focused on determining the change in the tank's SoC as a function of the heat loss to the environment by calculating U_t for a period of 16 h. Fig. 7a presents the prediction of U_t using real data through X-TFC and three other well-known experimental correlations. As demonstrated, the X-TFC framework is capable of predicting U_t for this type of problem with a relative error below 0.01 % (Fig. 4a and 4c). U_t is overpredicted by the Hilpert and Churchill-Berstein correlations in the 16-hour time horizon. This overprediction leads to relative errors that could be larger than 100 % with respect to the prediction obtained from X-TFC (see Fig. 7b). Among the correlations, Zukauskas demonstrated better performance for this problem, but still led to overprediction of U_t for most of the analyzed range (see Fig. 7a). An inaccurate HTC prediction will produce unreliable results in thermal system model evaluation. Fig. 7c demonstrates that important differences in the SoC of the thermal energy storage tank can be retrieved through an inverse problem analysis using heat loss information. The real SoC was accurately determined through X-TFC method during the 16-hour time span with maximum errors around 0.1 % (see Fig. 7d), outperforming any prediction obtained through the experimental correlations.

6. Conclusions

We developed a physics-informed ML model, X-TFC, to predict the HTCs and energy efficiency of thermal energy systems, addressing the limitations of the classical system modeling approach based on the use of empirical correlations. By employing the minimalistic structure of shallow random-projection neural networks and the time-domain decomposition, this method is capable of predicting highly variable thermal plant operational parameters and HTCs for very long operation times, achieving outstanding accuracy with an exceptionally low computational cost. We tested the accuracy and robustness of this physics-based model by using highly variable real weather condition data as the input. The model generated the tank temperature for 7 days of plant operation in just a few seconds of computational time, proving its capability to perform predictions for even longer time domains with great ease. In addition, this feat was achieved without propagation of error, as the algorithm is iterated at each subdomain and new initial conditions are updated accordingly with each new set of data. After testing the ability of the framework to estimate the HTCs and energy efficiency, we further validated the model on a real thermal energy storage tank in a concentrating solar power plant, obtaining relative

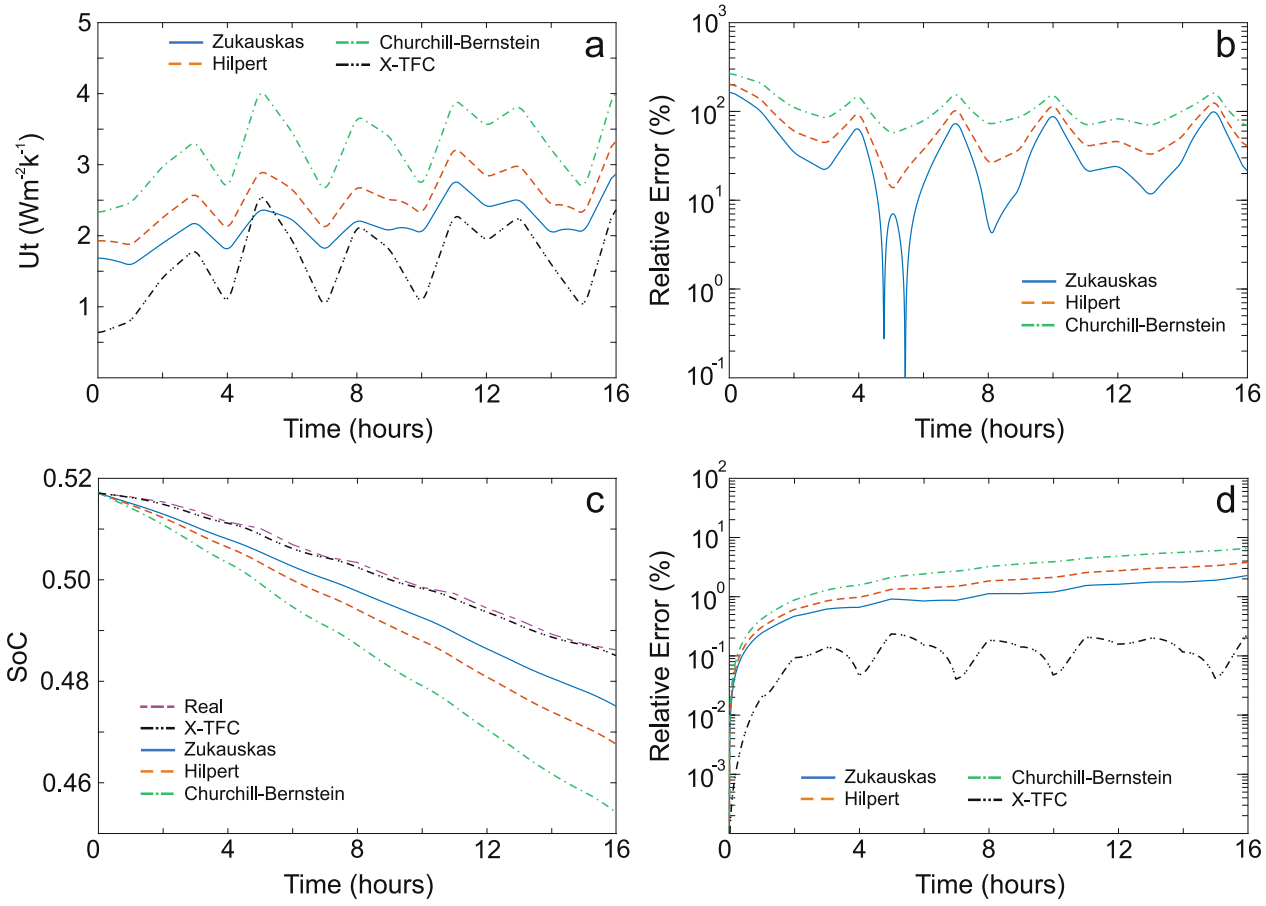

Fig. 7. (a) – (b) Experimental correlations led to an overprediction in the heat transfer coefficient U_t between a molten salt thermal energy storage tank and the environment, when compared with the X-TFC framework. (c) and (d) The state-of-charge of the tank was accurately retrieved by the X-TFC framework through the inverse problem analysis leading to relative errors below 0.1% and outperforming the predictions obtained through experimental correlations.

errors on the order of 0.1 %. Unlike other data-driven ML models such as gated recurrent units and transformers, our framework does not require offline training with historical data. Instead, it leverages the engineering knowledge of the underlying thermal plant in the form of a physics-based model, such as a differential equation model of the physical system. This not only allows us to perform online, real-time prediction of the system given certain input data, such as weather conditions, but also allows us to perform the same estimation for different thermal plants, as long as the physics-based model is adjusted accordingly. This capability makes this framework versatile and adaptable to different real-world energy systems. The flexibility of this framework also allows for modeling systems under real operation conditions, including the performance reduction caused by the deterioration of the system due to surface wear and corrosion, loss of insulation, pressure loss, and so on, during operation by considering the variation in the design and operation parameters. For instance, the proposed framework could be used to evaluate the performance of parabolic trough receivers as a function of the pressure variation due to imperfections in sealings, deterioration of the system, or hydrogen buildup during operation [39].

We conducted further validation on a real molten nitrate salt thermal energy storage tank in a 50-MW concentrating solar power plant, where X-TFC predicted heat transfer coefficient between the tank and the environment over a 16-hour period. By solving the differential equation with the heat transfer coefficients predicted by X-TFC, we achieved a tank temperature profile that closely aligned with the observed data, with a relative error below 0.1 %. This result demonstrates the efficiency of the framework in handling real plant data, and provides a substantial improvement over traditional experimental correlations, which tend to overestimate the heat transfer coefficient and produce less accurate temperature profiles.

CRediT authorship contribution statement

Julian D. Osorio: Writing – original draft, Conceptualization, Methodology, Validation, Formal analysis. **Mario De Florio:** Writing – original draft, Visualization, Validation, Software, Investigation, Formal analysis. **Rob Hovsapian:** Writing – review & editing, Resources, Methodology, Conceptualization. **Chrys Chryssostomidis:** Writing – review & editing, Conceptualization. **George Em Karniadakis:** Writing – review & editing, Methodology, Formal analysis, Conceptualization.

Declaration of competing interest

The authors declare that they have no known competing financial interests or personal relationships that could have appeared to influence the work reported in this paper.

Acknowledgements

This work was authored in part by the National Renewable Energy Laboratory, operated by Alliance for Sustainable Energy, LLC, for the U. S. Department of Energy (DOE) under Contract No. DE-AC36-08GO28308. This research was partially supported by U.S. Department of Energy Solar Energy Technologies Office (SETO) under the agreement 38475 and the Center for Energy Conversion and Storage Systems at National Renewable Energy Laboratory (NREL). The views expressed in the article do not necessarily represent the views of the U.S. Department of Energy (DOE) or the U.S. Government. The U.S. Government retains and the publisher, by accepting the article for publication, acknowledges that the U.S. Government retains a nonexclusive, paid-up, irrevocable, worldwide license to publish or reproduce the published form of this work, or allow others to do so, for U.S. Government purposes.

Appendix A

The geometric and physical parameters for the solar-thermal system analyzed in this study are presented in Table A1 [25,40].

Table A1
Geometric and physical parameters for the solar-thermal system [25,40].

Parameter	Value
Parabolic trough collector	
Receiver module length, L_m (m)	4.06
Number of modules,n	60
Total collector length, nxL_m (m)	243.6
Absorber inner diameter, $2r_1$ (mm)	66.0
Absorber outer diameter, $2r_2$ (mm)	70.0
GE outer diameter, $2\,r_4$ (mm)	115.0
GE thickness, $r_4 - r_3$ (mm)	3.0
Rim angle, ϕ_r (rad)	1.3963
Volume flow rate, $\dot{V}$ (m^3/s)	0.0063
Thermal energy storage	
Tank's surface area, A_t (m^2)	3,150
Tank volume, V (m^3)	18,343
Minimum tank temperature, T_∞ (K)	298
Maximum tank temperature, T_{max} (K)	673
Tank pressure, p_t (kPa)	101
Power generation cycle	
Effective conductance ratio, rM	1.0
Power ratio,$\dot{W}_p/\dot{W}_t$	0.05
Turbine's isentropic efficiency,η_t	0.9
Pump's isentropic efficiency,η_p	0.8
Equivalent conductance, $(UA)_{eq}$ (kW/K)	25
Relative heat leak,$\dot{Q}_{lk}/\dot{Q}_{max}$	0.01

Solar collector model

The solar radiation reflected in the collector mirror passes through the glass envelope, the annular gap, and gets absorbed in the absorber pipe, and

then is transferred by conduction to the HTF flowing inside. The heat transferred to the HTF, Q_{in} (W), can be calculated as the heat reaching the external surface of the absorber, $Q_r = IA_{ap}\eta_0\tau\alpha$, minus the thermal losses, i.e.:

$$Q_{in} = IA_{ap}\eta_0\varphi\alpha - Q_{l,c} \tag{A1}$$

where I (Wm^{-2}), A_{ap} (m^2), φ, and α are the solar irradiance, collector aperture area, glass envelope transmittance, and absorber pipe absorptance, respectively. The optical efficiency (η_0) is computed from Eq. A(2), where ξ_{cl} is the mirror reflectance, γ is the intercept factor, and K_θ is the incident angle modifier. Detailed information on the approach to calculate this ξ_{cl}, γ, and K_θ can be found in Duffie et al. [40].

$$\eta_0 = \xi_{cl}\gamma K_\theta \tag{A2}$$

The collector efficiency (η_c) is calculated as the ratio of Q_{in} and the total solar energy reaching the external surface of the PTC receiver (the glass envelope):

$$\eta_c = \frac{Q_{in}}{IA_{ap}} \tag{A3}$$

Rankine cycle model

The parameter *rM* corresponds to an effective conductance ratio between dissipation and input heat exchangers (Eq. A(4)). It also relates the fluid's specific heat and the mass flow rates for the low-temperature (designated with "*L*" subscript) and high-temperature (designated with "*H*" subscript) heat exchangers. The term *NTU* is the number of transfer units for each heat exchanger [25]:

$$rM = \frac{(\dot{m}c_p)_L(1 - e^{-NTU_L})}{(\dot{m}c_p)_H(1 - e^{-NTU_H})} \tag{A4}$$

The term η_{eq} in Eq. (12) considers the irreversibilities in the expansion and compression processes [25]:

$$\eta_{eq} = \frac{\eta_{i,t}\left(1 - \frac{W_p}{W_t}\right)}{1 - \eta_{i,t}\eta_{i,p}\frac{W_p}{W_t}} \tag{A5}$$

where W_p and W_t correspond to the power consumed in the pump and the power generated in the turbine, respectively. The $\frac{W_p}{W_t}$ in Eq. A(5) corresponds to the fraction of power produced in the turbine that is necessary to run the pump, which is about 5 % in a Rankine cycle.

Data availability

Data will be made available on request.

References

[1] Lovegrove K, Stein W. Concentrating Solar Power Technology: Principles, Developments, and Applications. 2nd Edition. Duxford, United Kingdom: Woodhead Publishing; 2020.

[2] Rohsenow W, Hartnett J, Cho Y. Handbook of Heat Transfer. 3rd Edition. New York, NY 10011: McGraw-Hill; 1998.

[3] Convection BA. Heat Transfer. 4th Edition. Hoboken, NJ: Wiley; 2013. 10.1002/9781118671627.

[4] Osorio JD, Wang Z, Karniadakis G, Cai S, Chryssostomidis C, Panwar M, et al. Forecasting solar-thermal systems performance under transient operation using a data-driven machine learning approach based on the deep operator network architecture. Energy Convers Manag 2022;252:115063. https://doi.org/10.1016/j.enconman.2021.115063.

[5] Wang J, Guo L, Zhang C, Song L, Duan J, Duan L. Thermal power forecasting of solar power tower system by combining mechanism modeling and deep learning method. Energy 2020;208:118403. https://doi.org/10.1016/j.energy.2020.118403.

[6] Vinuesa R, Brunton SL. Enhancing computational fluid dynamics with machine learning. Nat Comput Sci 2022;2:358–66. https://doi.org/10.1038/s43588-022-00264-7.

[7] Ranade R, Gitushi K, Echekki T. Generalized Joint Probability Density Function Formulation inTurbulent Combustion using DeepONet 2021.

[8] Lin C, Li Z, Lu L, Cai S, Maxey M, Karniadakis GE. Operator learning for predicting multiscale bubble growth dynamics. J Chem Phys 2021;154. https://doi.org/10.1063/5.0041203.

[9] Suh Y, Bostanabad R, Won Y. Deep learning predicts boiling heat transfer. Sci Rep 2021;11:5622. https://doi.org/10.1038/s41598-021-85150-4.

[10] Zhan T, Fang L, Xu Y. Prediction of thermal boundary resistance by the machine learning method. Sci Rep 2017;7:7109. https://doi.org/10.1038/s41598-017-07150-7.

[11] Wu Y-J, Fang L, Xu Y. Predicting interfacial thermal resistance by machine learning. NPJ Comput Mater 2019;5:56. https://doi.org/10.1038/s41524-019-0193-0.

[12] Clark Di Leoni P, Lu L, Meneveau C, Karniadakis GE, Zaki TA. Neural operator prediction of linear instability waves in high-speed boundary layers. J Comput Phys 2023;474:111793. https://doi.org/10.1016/j.jcp.2022.111793.

[13] Karniadakis GE, Kevrekidis IG, Lu L, Perdikaris P, Wang S, Yang L. Physics-informed machine learning. Nat Rev Phys 2021;3:422–40. https://doi.org/10.1038/s42254-021-00314-5.

[14] Chen J, Xu X, Zhou J, Li B. Interfacial thermal resistance: Past, present, and future. RevModPhys 2022;94:025002. https://doi.org/10.1103/RevModPhys.94.025002.

[15] Schiassi E, Furfaro R, Leake C, De Florio M, Johnston H, Mortari D. Extreme theory of functional connections: A fast physics-informed neural network method for solving ordinary and partial differential equations. Neurocomputing 2021;457:334–56. https://doi.org/10.1016/j.neucom.2021.06.015.

[16] De Florio M, Schiassi E, Furfaro R. Physics-informed neural networks and functional interpolation for stiff chemical kinetics. Chaos: An Interdisciplinary Journal of Nonlinear Science 32(6), 063107, 2022.

[17] Osorio JD, Rivera-Alvarez A. Performance analysis of Parabolic Trough Collectors with Double Glass Envelope. Renew Energy 2019;130:1092–107. https://doi.org/10.1016/j.renene.2018.06.024.

[18] Gnielinski V. New equations for heat and mass transfer in the turbulent flow in pipes and channels. Int Chem Eng 1975;16:359–63.

[19] Dittus FW, Boelter LMK. Heat Transfer in Automobile Radiators of the Tubular Type. Int Comm Heat Mass Transfer 1985;12:3–22.

[20] Sieder EN, Tate EC. Heat transfer and pressure drop of liquids in tubes. Ind Eng Chem 1936;28:1429–36.

[21] Bergman TL, Lavine AS, Incropera FP, DeWitt DP. Introduction to Heat Transfer. 6th Edition. Hoboken, NJ: Wiley & Sons; 2011.

[22] Žukauskas A. Heat Transfer from Tubes in Crossflow 1972:93–160. https://doi.org/10.1016/S0065-2717(08)70038-8.

[23] Hilpert R. Forsch Geb. Ingenieurwes . vol. 4. 1933.

[24] Churchill SW, Bernstein M. A Correlating Equation for Forced Convection From Gases and Liquids to a Circular Cylinder in Crossflow. J Heat Transfer 1977;99:300–6. https://doi.org/10.1115/1.3450685.

[25] Osorio JD, Rivera-Alvarez A, Abakporo OI, Ordonez JC, Hovsapian R. Thermodynamic Modeling of Heat Engines Including Heat Transfer and Compression–Expansion Irreversibilities. J Therm Sci Eng Appl 2022;14. https://doi.org/10.1115/1.4050786.

[26] Andreas A, Stoffel T. NREL Solar Radiation Research Laboratory (SRRL): Baseline Measurement System (BMS). CO, USA: Golden; 1981.

[27] Rivera-Alvarez A, Osorio JD, Montoya-Duque L, Fontalvo J, Botero E, Escudero-Atehortua A. Comparative analysis of natural gas cogeneration incentives on

electricity production in Latin America. Energy Policy 2020;142:111466. https://doi.org/10.1016/j.enpol.2020.111466.
[28] Mortari D. The Theory of Connections: Connecting Points. Mathematics 2017;5:57. https://doi.org/10.3390/math5040057.
[29] Osorio JD, Rivera-Alvarez A. Influence of the concentration ratio on the thermal and economic performance of parabolic trough collectors. Renew Energy 2022; 181:786–802. https://doi.org/10.1016/j.renene.2021.09.040.
[30] Osorio JD, Zea S, Rivera-Alvarez A, Patiño-Jaramillo GA, Hovsapian R, Ordonez JC. Low-temperature solar thermal-power systems for residential electricity supply under various seasonal and climate conditions. Appl Therm Eng 2023;232:120905. https://doi.org/10.1016/j.applthermaleng.2023.120905.
[31] De Florio M, Kevrekidis IG, Karniadakis GE. AI-Lorenz: A physics-data-driven framework for Black-Box and Gray-Box identification of chaotic systems with symbolic regression. Chaos Solitons Fractals 2024;188:115538. https://doi.org/10.1016/j.chaos.2024.115538.
[32] Ahmadi Daryakenari N, De Florio M, Shukla K, Karniadakis GE. AI-Aristotle: A physics-informed framework for systems biology gray-box identification. PLoS Comput Biol 2024;20. https://doi.org/10.1371/journal.pcbi.1011916. e1011916.
[33] Nath K, Meng X, Smith DJ, Karniadakis GE. Physics-informed neural networks for predicting gas flow dynamics and unknown parameters in diesel engines. Sci Rep 2023;13:13683. https://doi.org/10.1038/s41598-023-39989-4.
[34] Carvalho F de CT, Nath K, Serpa AL, Karniadakis GE. Learning characteristic parameters and dynamics of centrifugal pumps under multi-phase flow using physics-informed neural networks. ArXiv:231003001 2023:1–38.
[35] Gawronska E, Zych M, Dyja R, Domek G. Using artificial intelligence algorithms to reconstruct the heat transfer coefficient during heat conduction modeling. Sci Rep 2023;13:15343. https://doi.org/10.1038/s41598-023-42536-w.
[36] Cho K, van Merrienboer B, Gulcehre C, Bahdanau D, Bougares F, Schwenk H, et al. Learning Phrase Representations using RNN Encoder-Decoder for Statistical Machine Translation 2014.
[37] Vaswani A, Shazeer N, Parmar N, Uszkoreit J, Jones L, Gomez AN, et al. Attention Is All You Need 2017.
[38] Guo H, Zang C, Wang Z, Zhao X, Meng Y, Osorio JD, et al. Analysis of thermal and mechanical properties with inventory level of the molten salt storage tank in central receiver concentrating solar power plants. Appl Therm Eng 2025;260: 124984.
[39] Vinuesa R, Luna M, Cachafeiro H. Simulations and experiments of heat loss from a parabolic trough absorber tube over a range of pressures and gas compositions in the vacuum chamber. *J Renewable Sustainable Energy* 2016;8:023701.
[40] Duffie JA, Beckman WA. Solar engineering of thermal processes. 4th Edition. Hoboken, NJ: John Wiley & Sons, Inc.; 2013.